Development of an intrusive core complex and early landsliding on Juana Ridge, Fernandina northwest submarine rift zone, Galápagos Archipelago

Jennifer Glass

University of Washington on

School of Oceanography

Box 357940

Seattle, WA 98195-7940

March 4, 2006

Advisors:

Prof. Mark Holmes, UW

Dr. Daniel Fornari, WHOI

Non-Technical Summary

A ~20-km-long submarine volcanic ridge off the northwestern coast of Fernandina Island, the westernmost of the Galápagos Archipelago, was studied aboard the University of Washington research vessel, the *Thomas G. Thompson*. The ridge, which I have named Juana Ridge, is a volcanic rift zone formed by movement of magma (magmatic "diking") in a northwesterly direction from the chamber underlying Fernandina Island. Juana Ridge was hypothesized to be dominated by an intermediate stage of development, characterized by the growth of an intrusive (coarse-grained and slowly-cooled) core at its near-shore end and abundant volcanic morphologies, such as cones and craters containing deep pits, along its axis. Multiple research methods were employed to determine properties of the seafloor, including sonar mapping to measure bathymetry and reflectivity (high for lava; low for sediment), magnetic field strength measurement and sub-bottom profiling for evidence of sediment cover. Growth of a solid rift zone core was verified by along-rift-axis and across-rift-axis slope profiles. Numerous cones and craters located along the rift axis and a double-dipole magnetic anomaly located over the near-shore end of the rift indicate a solid core still in the process of cooling. Not predicted by the hypothesis was the discovery of two large (several square kilometer) landslide blocks, possibly formed by slope failure due to severe steepening of rift-axis flanks during growth of the core complex. The presence of a deep field (~3000 m) of abundant deep-pitted craters off the northern tip of the rift zone, correlated with areas of very high reflectivity (lava) in backscatter, was also unexpected. These flows may have formed due to magma withdrawal from the volcanic summit during the catastrophic caldera collapse of Fernandina Volcano in 1968, and eruption in the deep portions of Juana Ridge.

Acknowledgements

I would like to express heartfelt appreciation for my two advisors, Professor Mark Holmes of UW School of Oceanography and Dr. Daniel Fornari of Woods Hole Oceanographic Institution. I also thank Professor Roy Carpenter for organizing the unique opportunity for undergraduate oceanographic research around the Galápagos Archipelago, and to the State of Washington for funding undergraduate research time aboard the R/V Thomas G. Thompson. I also thank Ms. Susan Atkins for financial and moral support. The instructors and teaching assistant of Oceanography 443 and 444 Autumn 2005 and Winter 2006 provided guidance, advice and careful paper editing: Professor Seelye Martin, Professor Gabrielle Rocap and Llyd Wells. I thank UW School of Oceanography Chair Professor Russell McDuff, Undergraduate Program Advisor Professor Rick Keil and the entire School of Oceanography for supporting undergraduate research in general and this cruise in particular. I would like to recognize Professor Miles Logsdon, Dr. Mimi D'Iorio and Jill Coyle of the UW School of Oceanography Spatial Analysis Laboratory for technical support and guidance. Professor John Delaney and Deborah Glickson of UW School of Oceanography Marine Geology and Geophysics provided useful discussions. Ecuador Armada (INOCAR) collaborator Lt. Giorgio de la Torre was very helpful during TN189 with data processing. Thank you to Captain Phil Smith and the crew of the R/V *Thomas G. Thompson* cruise TN189 Leg 1, especially marine technician Robert Hagg. Dr. Scott White of University of Southern Carolina provided additional EM300 data from TN188 for use in my project. Thanks to WHOI scientists Dr. Maurice Tivey and Dr. Adam Soule, University of Idaho Professor Dennis Geist and Monterey Bay Aquarium Research Institution scientist Dr. Dave Clague for technical scientific guidance and helpful discussions. My family (Sara, Geoffrey and Rachel Glass) was supportive and encouraging throughout these six months of work. And last but not least, thanks to my colleagues and classmates in Oceanography 443 and 444, especially Wesley Thompson, Heidi Berkenbosch and Hillary Hall, and to the scientific party of TN189, both Seattleites and Ecuadorians.

Abstract

The ~20-km-long northwest submarine rift zone of Fernandina Island, Galápagos Archipelago, hereafter referred to as Juana Ridge, was explored with high resolution (EM300) swath mapping, surface magnetic measurements and 3.5 kHz sub-bottom profiling aboard the R/V *Thomas G. Thompson*. Juana Ridge was hypothesized to be in a developmental stage corresponding to the growth of an intrusive core complex and accompanied by abundant axial volcanism. Intrusive core growth was supported for the region from the shoreline to 10-15 km down-rift by along-axis and across-axis profiles and by magnetic anomaly data. The latter characterized the magnetic signature of Juana Ridge as a double-dipole with a negative anomaly (-2000 nano-Teslas) over the axis. Backscatter data indicated prominent high-reflectivity distal deep lava flows which correlate geographically with a pit crater field at ~3000 m water depth. The eruption of these pit craters and low-angle distal flow may have been the effect of the 1968 caldera collapse on Fernandina Island and subsequent magma withdrawal, resulting in the displacement of magma to the deep regions of Juana Ridge, and reinvigorating distal low-angle lava flows. Sediment cover was found to be very low in the study area, except possibly in the region of the deep distal flows, indicating recent rift zone volcanism. Two prominent landslide slump blocks of several square kilometers were identified on the south flanks of Juana Ridge, requiring reconsideration of the assumption that Hawaiian models of rift zone growth and late-stage mass wasting can be accurately applied to Galápagos submarine rift zones.

Introduction

The Galápagos Islands are believed to result from upwelling of a hot magma plume from the deep mantle. Such "hot spot" volcanism differs in both composition and eruptive style from that of subduction-source continental volcanism (e.g., the Andes and the Cascades). Hot spot volcanic islands are generally built of lavas lower in silica, and thus lower in viscosity, than continental arc volcanoes, generating low-slope, massive shield volcanoes found in oceanic hot-spot provinces such as Hawaii and the Galápagos Archipelago. The volcanic islands of the Galápagos are characterized by a distinct shape, thought to resemble "over-turned soup bowls," controlled by circumferential fissures surrounding central calderas. The youngest islands in the Galápagos Archipelago are located in the west, due to spreading at the East Pacific Rise moving the Nazca Plate in an eastward direction over the "fixed" Galápagos Hot Spot.

The westernmost island in the Galápagos Archipelago, Fernandina Island (Fig. 1, 2), is located over the leading edge of the Galápagos Hot Spot (Kurz and Geist 1999) and has the typical Galápagos soup-bowl shape. Its central caldera is believed to overlie a shallow, flat-topped, diapiric magma chamber (Chadwick and Dieterich 1995, Allan and Simkin 2000; Fig. 2). The most active volcanic island in the Galápagos Archipelago, Fernandina Island erupts on average once every several years (most recently in 2005). The largest documented eruption was in 1968, accompanied by a caldera collapse in which the caldera floor dropped an estimated 300 m (Simkin and Howard 1970; Fig. 3).

While the sub-aerial portions of oceanic hot-spot islands are more accessible and thus more-often studied, submarine rift zones are the building blocks of oceanic hot-spot shield volcanoes and hot-spot platforms. Their formation depends on lateral propagation of dikes from a central volcanic magma chamber (Fiske and Jackson 1972). It is often the case that sub-aerial and submarine rift zones are continuous. On Fernandina Island, a broad topographic ridge with an average slope of 5º, containing abundant radial fissures, is located on the northwest sector of Fernandina Island (Chadwick and Howard 1991, Rowland 1996; Fig. 2). (Hereafter this feature will be referred to as the Fernandina Northwest Rift Zone (FNWRZ) (Fig. 2)). FNWRZ is the sub-aerial expression of the more-distinct submarine ridge originating at Capo Douglas and continuing ~20 km northwest of Fernandina Island to water depths of ~3000 m. The ridge has a prominent bend at ~1700 m water depth at Km 10 (with "Km" defined as the length along-axis measured from Capo Douglas) from a 310º to 350º strike (Fig. 2). Multibeam bathymetry data

collected during the NEMO-2 cruise on the *R/V Melville* in 2000 (Kurz et al. 2000) and the DRIFT Leg-4 cruise on the *R/V Roger Revelle* in 2001 (Kurz et al. 2001, Harpp et al. 2003) characterized this ridge as a submarine rift zone due to abundant constructional volcanic morphologies, such as pit craters and volcanic cones, along the ridge's axis and flanks. Hereafter, this feature will be referred to as Juana Ridge, to commemorate the only heiress of Ferdinand V and Isabella I of Spain, after whom the two westernmost Galápagos islands were named, and thus to exemplify the volcanic ancestry of this hot-spot rift zone. Juana Ridge represents the propagation of the Galápagos Hot Spot into the as-yet-undisturbed oceanic crust of the Nazca Plate underlying the Pacific Ocean west of the Galápagos Archipelago (Fig. 2).

A relevant submarine rift zone analogue to Juana Ridge is the well-studied 75-km-long Puna Ridge, the submarine continuation of the Kilauea East Rift Zone (KERZ) into the Pacific Plate east of Hawaii. Both Juana and Puna Ridges were created by lateral diking of magma chambers underlying Fernandina Island and Kilauea, respectively. However, it has been noted (e.g. Kurz et al. 2000, Rowland 1996) that in contrast to the prominent KERZ (with a narrow width of 2-3 km), the sub-aerial FNWRZ is relatively diffuse (~5-6 km wide (Fig. 2)) and lacks KERZ's volcanic features, such as pit craters, grabens and open fractures. Rowland (1996) attributes this to the developmental immaturity of FNWRZ relative to KERZ.

In this study I test the hypothesis that Juana Ridge is in a more juvenile state of development than Puna Ridge. Stephen Leslie and colleagues (Leslie et al. 2004) have developed a useful model for submarine volcanic rift zone evolution that divides a submarine rift zone into three distinct domains, each of which can be correlated with temporal developmental rift-zone stage. Stage/Domain 1 is characterized by voluminous sheet flows at the rift zone's distal end (Fig. 4). Stage 2 begins when the pile of sheet flows (Domain 1) reaches a height that favors dike intrusion, providing the rift zone a well-developed slope of ~6° and favoring vertical growth by rift-zone eruptions (Domain 2) (Fig. 4). The third and final stage of rift-zone growth is indicated by a decrease in slope to ~3° and a widening of the dike intrusive zone (Domain 3), accompanied by surficial mass wasting (Fig. 4).

It is thus predicted that a mature rift zone in the third stage of development will maintain a constant slope for most of its length. This prediction is consistent with modeling experiments showing that the evenness of a volcanic ridge's slope is an indication of the continuity of the underlying intrusive dike complex (Fialko and Rubin 1999). A steeper, more variable along-axis

rift-zone profile is predicted by models of shorter dike systems and those with low magmatic driving pressure (Fialko and Rubin 1999). In accordance with the model of a continuous dike complex, Puna Ridge maintains an extremely constant 2.9º slope from the coastline to Km 45 (2700 m depth), where it plunges more steeply at ~6º (Lonsdale 1989, Smith et al. 2002). Thus, Puna Ridge is thought to be dominated by Stage/Domain 3-type volcanic rift zone growth to a depth of ~2700 m, where Stage/Domain 2 begins to dominate (Leslie et al. 2004). This is consistent with magnetic surveys that have identified a dike complex 4-5 km in width underlying the proximal ~70 km of the ridge (Malahoff and McCoy 1967, Leslie et al. 2004), to a depth of ~4500 m where Domain 1 (distal rift-zone submarine lava flows) begins to dominate (Holcomb et al. 1988, Leslie et al. 2004).

Juana Ridge's along-axis slope has been previously measured to average ~9° (Kurz et al. 2001, Harpp et al. 2003) out to Km 10. This slope is higher than predicted for Domain 2 of the Leslie et al. (2004) model (6°) and was re-calculated from high-resolution EM300 bathymetric data in the work reported here. Across-axis slope profiles (calculated previously at 15-50° (Kurz et al. 2001)), much steeper than the 8-12° across-axis slopes measured for Puna Ridge (Lonsdale 1989)) were also re-calculated at both the proximal and distal ends of Juana Ridge. It was predicted that slopes would be steeper at the proximal end of Juana Ridge if an intrusive core complex is developing from the proximal end outwards. Also predicted by employing the Stage 2 of Leslie et al. (2004) model were that (1) high-resolution bathymetric data would reveal most constructional volcanic morphologies to be focused along and slightly off-axis of Juana Ridge, as recognized by previous mapping efforts (Fornari et al. 2001, Kurz et al. 2001); (2) high-resolution bathymetric data would not show mass wasting scarps and other erosional, late-stage rift-zone developmental features; (3) backscatter and sub-bottom profiling data would show sediment aerial extent and thickness to be greater on the distal flows left-over from Stage 1 of the Leslie et al. (2004) rift-zone propagation model than on Juana Ridge; and (4) magnetic data would reveal a magnetic anomaly over proximal portion of Juana Ridge, indicative of a magnetized intrusive core complex. High resolution swath mapping, surface magnetic measurements and 3.5 kHz sub-bottom profiling were employed during Leg 1 of R/V *Thomas G. Thompson* cruise TN189 (12-20 January 2006) to test my hypothesis that Juana Ridge is dominated by developmental Domain/Stage 2 of the Leslie et al. (2004) model.

Methods

Field Work

On Leg 1 of TN189 a study area of approximately 324 km^2 was mapped, from 91°50' W to 91°40' W longitude and from 0°10' S to 0°20' S latitude (Table 1, Fig. 5). Mapping was conducted at 7 knots for 170 kilometers of track-lines (10 track lines total) over a 17.5 hour period (Table 1, Fig. 5). Geo-referenced bathymetry and co-referenced amplitude (backscatter) data were collected using the Kongsberg Simrad 30 kHz EM300 multi-beam sonar system. The EM300 system transmits a 135° beam (135 individual 1° (vertical) and 2° (horizontal) beams), with a bottom depth error of <0.2% water depth (for this survey between 300-3000 m, the error is 0.6-6 m depending on water depth). Sound velocity for the EM300 system was corrected with a CTD (Conductivity-Temperature-Depth) cast to ~3300 m (Table 1). Position correction was made by P-Code GPS and motion-sensing correction was made by POS/MV Model 320. EM300 data were displayed and recorded using MB System® software.

A Knudsen 3.5 kHz sub-bottom profiler was used to determine sediment thickness and relative lava-roughness. The sub-bottom profiler system consisted of a Knudsen 320R transceiver, with maximum output power of 10 kW, that swept through a band of frequencies between 2-7 kHz with a nominal frequency of 3.5 kHz. This system employs a total of 12 Massa TR-109A units in a 3 x 4 array, resulting in an effective beam width of approximately 30°. The area of the Fresnel zone (the circular path of seafloor insonified) ranged from 2 km^2 at 3000 m to 200 m^2 at 300 m water depth, resulting in a resolution ~3% that of the EM300 system. The normal settings were a 1000 m or 500 m depth window, an output power of 5 kW, and a chirp pulse length of 6 or 12 msec. The data were displayed in real time on a computer monitor and were also recorded on an EPC 9800 thermal graphic recorder.

A Marine Magnetics® SeaSPY marine magnetometer (sensitivity of 0.01 nano-Teslas (nT) and an absolute accuracy of 0.2 nT) was towed 250 m behind the ship at 50 m water depth throughout the survey, at cycling rate of 1 second, to measure the magnitude of the magnetic field. The data were displayed and recorded using SeaLINK software. The position of the magnetometer was determined by inserting an offset of 250 m to the GPS-derived vessel position, which in turn was corrected for the distance between the A-frame (meter wheel) and the GPS-receiving antenna.

Post-Cruise Analyses

Bathymetric data were cleaned and merged using CARIS® HIPS and SIPS software. Data were gridded at 25 m and displayed using Interactive Visualization System® Fledermaus visualization software, which was used to make cross-sectional profiles. Grazing-angle corrections were made for backscatter data using CARIS® HIPS and SIPS software, gridded at 25 m and displayed using Interactive Visualization System® Fledermaus visualization software. Magnetic data were checked for diurnal magnetic variations using Microsoft® Excel software and displayed in Interactive Visualization System® Fledermaus visualization software. Regional field strength (the 2005 International Geomagnetic Reference Field (IGRF)) was subtracted from the raw magnetic data using Matlab® software, with .mat and .m files provided by Dr. Maurice Tivey of Woods Hole Oceanographic Institution, to generate a magnetic anomaly map.

Results

Dimensions and Slope Profiles

High resolution (25 m) EM300 bathymetry data show Juana Ridge to be a 20-km-long, ~8-km-wide (tapering to its distal end) feature with a prominent trend change from 310° to 350° at Km 10 outwards from its proximal end (Fig. 6). The slope was found to be quite variable, ranging from 9-10° at the proximal end (Figs. 6, 7a), averaging 4-5° down to the distal end of the rift zone (~2500 m water depth), with a deep section between 2100-2300 m of 11-12° (Figs. 6, 7b). Across-axis slope profiles were measured at both the proximal and distal ends of Juana Ridge. Slopes were found to be steeper (18-19°) on the southern slopes for the proximal end profile (across-axis) than the northern slopes (13-14°) (Figs. 6, 7c). The proximal-end rift zone axis was found to be well-defined (Fig. 7c). The distal end across-axis profile showed an irregular axis with fairly symmetrical side-slopes (~14°) (Fig. 6, 7d).

Sub-bottom Profiles

Sub-bottom profiles were characterized by parabolic reflections with little-to-no indication of sediment, except for several isolated areas of < 5 m of sediment at the very distal end of the Juana Ridge. Parabolic reflections across the rift zone likely indicate rough magma flows of pillow basalt morphology (Fig. 8).

Volcanic and Tectonic Morphologies

Examination of EM300 bathymetry revealed numerous volcanic morphologic features (Fig. 9, inset A). On the south flank of the proximal end of Juana Ridge, these included one 600-m-diameter cone with ~25° side slopes, a field ~2 km in length and 1 km in width with abundant (~10) craters averaging ~100 m in diameter with 10-20 m deep pits, and a slump feature (1 km x 500 m) with a ~25° western side slope and a 20° eastern side slope. Approximately 1 km west of the strike-change (at Km 10 and 1700 m water depth) lies a 1 x 2 km slump block with ~25° side slopes. Approximately 500 m northwest of this feature lies an isolated ensconced pit crater 200 m in diameter and 30 m deep (Fig. 9, inset B). Approximately 2 km north of the slump block lie two large pit craters ~400 m in diameter and 80-100 m deep (Fig. 9, inset C). At the distal end of Juana Ridge is a pit crater field ~ 4 x 7 km containing ~10 pit craters with an average diameter of ~200 m and an average depth of ~50 m (Fig. 9, inset D). The remainder of Juana Ridge is composed of an irregular surface indicative of lava flows and terraces (Fig. 9).

Backscatter

Backscatter data revealed two prominent lava-flow fields of high reflectivity (dark gray in backscatter shading) at the distal end of Juana Ridge (Fig. 10). The western flow field is approximately 8 km in length and 2 km in width. The eastern flow field is approximately 5 km in length and 2 km in width. These two flow fields directly overlie the pit crater field at the distal end of Juana Ridge (Fig. 9, inset D).

Magnetic Anomaly

The magnetic anomaly map shows a clear negative magnetic anomaly over the rift zone (Fig. 11). The proximal-end is < -2000 nano-Teslas (nT). The anomaly decreases radially outward, following a strike of ~310°, with no apparent strike change at the 1700 m, Km 10 strike-change bend in Juana Ridge's bathymetry (Fig. 11). The zero-anomaly contour line approximately follows the 2500 m depth contour. Positive anomalies (up to > +500 nT) are located to the northeast and southwest of the proximal end of Juana Ridge, forming a double dipole across the proximal end of Juana Ridge (Fig. 11).

Discussion

Juana Ridge's along-axis slope has been recalculated with EM300 bathymetric data and found to be more variable than the average ~9° slope calculated in previous surveys (Kurz et al. 2001, Harpp et al. 2003). The variability of slope in the first 10 km of Juana Ridge is evidence for an oversteepened dike complex underlying only the proximal ~2.5 km of Juana Ridge where slopes reach 6-10° (Fig. 7a). Variable yet low along-axis slopes of 2-6° from Km 2 down to Km 15 (2100 m water depth) likely indicate the initial development of a dike complex at these depths (Fig. 7a, b). There is a great steepening of slope from 2100-2300 m water depth (Km 15) to 11-12° (Fig. 7b). Similar distal-end slope-steepening occurs on Puna Ridge at a water depth of 2700 m (from 3 to 6°). In the case of Puna Ridge, this is likely concurrent with the transition from Domain 3 to Domain 2. However, at Juana Ridge the slope steepening is much too great to be related to such a process, which would also require the slope to decrease as it transitioned from Domain 2 to 1. The slope steepening may be due to the effect of the critical pressure of seawater on eruptive processes. At deep depths, seawater will not expand as much with the same amount of heating and thus will not promote the explosive volcanism that is produced at shallower depths and accommodates lower along-axis slopes (Moore and Chadwick 1995).

Across-axis slope profiles show clear evidence for the development of an oversteepened intrusive core at the proximal end of Juana Ridge (Fig. 7c, d). The proximal across-axis profile shows a well-developed rift axis indicative of an intrusive core complex, whereas the distal across-axis profile shows an irregular axis with no indication of an intrusive core complex (Fig. 7c, d). The origin of steeper proximal southern (18-19°) than northern slopes (13-14°) may be due to current volcanic activity on the southern slopes, although the nature of this asymmetry in volcanic foci is unknown. Across-axis slopes were similar (~15°) to those calculated by previous studies (Kurz et al. 2001, Harpp et al. 2003), although the high slopes (up to 50°) reported in those studies were not found to be statistically significant over the length of the rift and are only present in localized, very-oversteepened areas. Juana Ridge across-axis slopes are quite similar, although overall slightly higher, than those of Puna Ridge (8-12°) (Lonsdale 1989). This may result from the recent development of an intrusive core complex at Juana Ridge and related oversteepening.

A sub-bottom profile along track-line 8 (Fig. 6, 8), across-axis at the proximal end, illustrates that the upper portion of the rift zone is steeper than the deeper portions. This is likely

due to oversteepening by development of a proximal intrusive core complex and abundant proximal volcanism. The profile shows parabolic reflections indicative of rough magma flows of pillow basalt morphology, with no or very little sediment cover (Fig. 8). Low sediment cover on the rift zone is consistent with Domain/Stage 2 volcanism.

High-resolution bathymetric data were expected to reveal most constructional volcanic morphologies focused along and slightly off-axis of Juana Ridge if Domain/Stage 2 of rift zone formation were dominant, due to concentrated upward growth of the rift zone by an intrusive core complex centered under the rift axis. A steep-sided (20-25°) 100-m-tall cone (~600 m in diameter) was identified just off-axis (south-side) at the very proximal end of the rift (Fig. 9, inset A). Just northwest of the cone was an on-axis field of ~10 craters (averaging 100 m in diameter) ranging in height from 20-80 m with ~10-20 m deep pits (Fig. 9, inset A). These volcanic morphologies are likely primary vents erupting from vertical dikes issuing from the intrusive core complex, resulting from a larger magma pressure than for lower-sloped terrace lava flows (Smith et al. 2002). Sharp-sided cones are evidence for gas-rich magmas, in accordance with dredged lavas from Juana Ridge that have been found to be gas-rich (Kurz et al. 2000). Craters with pits likely formed by magma withdrawal, once a blocked down-rift passage was breached, allowing for magma drain-back (Lonsdale 1989, Smith et al. 2002).

The number and size of pit craters increases with distance along the rift zone. Two large pit craters (200 m in diameter with 30 m deep pits) each ~150 m tall are located at approximately Km 12, just west of the bend in the rift zone at Km 10 (Fig. 9, inset C). A similar abundance of pit craters is associated with the kink in Puna Ridge at Km 45 from a 65° to 45° strike, and has been attributed to the impediment in the down-rift flow of magma by the rift bend (Lonsdale 1989).

A field of ~10 pit craters with average heights of 50 m, each approximately 200 m in diameter, has been identified at the very distal end of Juana Ridge (~3000 m water depth). This pit crater field exactly overlies two prominent high reflectivity distal lava-flow fields apparent in the backscatter map, covering an area of approximately 20 km^2 (Fig. 10). Such low-angle distal lava flows are likely Stage/Domain 1 features, resulting from long-distance lateral propagation of dikes from the magma chamber underlying Fernandina Island. These deep lava flows have been previously identified (Fornari et al. 2001, Kurz et al. 2001), but appeared joined in previous studies. In the present study, these two flow fields are distinctly separated by a sediment (light

gray) strip (Fig. 10). Since only five years have passed since the previous study, it appears that the sedimentation rate is quite high in this region. Thus, the > 50% sediment cover identified on a previous deep-sea camera tow survey (Kurz et al. 2001) may not preclude recent (~50 years ago) eruption of these deep-sea lava flows. It has previously been suggested (e.g. Fornari et al. 2001) that these flows may have been the result of magma withdrawal and deep-sea eruption after the 1968 Fernandina caldera collapse, similar to the suggestion that distal flows off of Puna Ridge were the result of the 1924 Kilauea caldera collapse (Holcomb et al. 1988). Low sediment cover is also support for recent volcanism on Juana Ridge, due to the very low sediment cover found in the sub-bottom profile record (Fig. 8). Sedimentation generally appears to be greater in the deeper regions of the study area, although shading differences are rather difficult to discern (Fig. 10).

Perhaps the most puzzling attribute of the data set is the clear presence of at least two slump blocks on the southern slopes of Juana Ridge (Fig. 9, inset A and B), when no mass wasting features were predicted to be occurring on such a presumably young ridge. One slump block (~1 km x 500 m) with a well-defined normal fault striking ~330° and dipping ~25° to the southwest, is present at the proximal end of Juana Ridge (~ Km 2) (Fig. 9, inset A). This slump was likely the result of oversteepening and faulting due to development of the proximal intrusive core complex because the fault lies approximately parallel to the rift zone. The second obvious slump block (~1 km x 2 km) is located at ~Km 9, very close to the bend at Km 10, and is the result of a down-dropped hanging wall with an interesting morphology (a ridge runs down the western side) (Fig. 9, inset B). The normal fault responsible for this mass wasting feature strikes ~5° and dips 25° to the northwest. Thus, this fault is nonparallel to the rift zone, which strikes ~310° at this depth. This slump, similar to the prominent pit craters just northwest of it, may have arisen due to excess stress related to the impediment of lava flow near the bend in the rift zone. Landslide features are present on Puna Ridge (Smith et al. 2001), although not in great abundance. In the Galápagos Archipelago, the only volcanic ridge landslides are those on Genovesa Ridge (Fig. 1). However, recent studies have revealed that Galápagos submarine landsliding to be more important than previously recognized (Cando 2006, Cougan 2006).

Magnetic data reveal a clear magnetic anomaly over the proximal portion of Juana Ridge, indicative of an intrusive core complex (Fig. 11). While topographic interferences may be a source of error, they are expected to be negligible with surface-towed magnetic studies. The

double-dipole nature of the anomaly, with positive anomalies to the northeast and southwest of the proximal end of the rift zone, is unexpected. This may be related to the magnetized intrusive core cooling from the outside in. If the cool outside of the core contains a higher magnetic signature than the warm inside, a double dipole can be produced. The magnitude of the magnetic anomaly is quite similar to that observed on Puna Ridge (Leslie et al. 2004), with a negative anomaly < -2000 nT and a positive anomaly (two in the case of Juana) > +500nT. In the case of Puna Ridge, the dipole is oriented normally (negative to the north, positive to the south). In the case of Juana Ridge, the magnetic anomaly follows the strike of the rift zone (310°) along the rift, but showed no sign of changing strike with the prominent bathymetric bend at Km 10. Thus, the intrusive complex creating the anomaly is presumed to be confined to the proximal end of the rift zone.

Conclusions

High resolution swath mapping, surface magnetic measurements and 3.5 kHz sub-bottom profiling of Juana Ridge revealed numerous lines of evidence for the development of an intrusive core complex underlying the proximal ~5-10 km of Juana Ridge. Along-axis bathymetric slope calculations indicate a well-defined underlying core complex down to Km 2, with the region between Km 2 and 15 containing a less-well-defined core, and perhaps only the beginnings of an intrusive complex. Across-axis slope profiles verify the presence of an intrusive core complex creating a well-defined rift axis profile at the proximal end of the rift (in depths shallower than Km 10, at the bend), whereas the regions deeper than Km 10 show an irregular cross-axial profile. Most constructional volcanic morphologies were located on or slightly off-axis (usually lying on the southern slopes). Shallow volcanic morphologies were dominated by cones and craters likely formed by higher gas content, whereas deeper volcanic morphologies were mainly pit craters, including two prominent pit craters at the Km 10 bend, and a field of pit craters at the very distal end of the rift zone, which correspond to a previously-studied 20 km^2 low-angle distal lava flow. This lava flow may have been erupted contemporaneously with the 1968 Fernandina caldera collapse, as previously suggested and supported by the high sedimentation rates construed from comparison of this study's backscatter data with that of a previous study 5 years ago. Two slump blocks on the southern flanks of Juana Ridge, each several square kilometers, indicate that mass wasting is occurring on Juana Ridge, possibly reflect oversteepening of rift

slopes from growth of the intrusive core complex. Magnetic anomaly mapping revealed a prominent double dipole that may indicate a still partially warm core complex, with the strongest negative anomaly centered over the axis of the rift zone.

The active nature of this rift zone is supported by sub-bottom profiling data, which failed to resolve sediment cover less than several meters, and identified no- to very-little sediment cover in the study area. While this may be due to lower sediment flux over the axis than in the deep distal area, it also suggests recent volcanism on Juana Ridge. A CTD tow-yo along the Juana Ridge rift axis between ~ Km 5-10 identified no hydrothermal signature in the water column down to depths of 20 above the bottom (Thompson 2006), but hydrothermal discharge may be sporadic or focused mainly at the proximal end of rift.

Another question posed by the high resolution EM300 bathymetry data set is the cause of the strike change at Km 10. It is possible that at this depth the dominant stress field changes from that of the direction preferred by lateral diking from the magma chamber under Fernandina Island to that of the regional stress field, possibly controlled by the volcano to the north of Juana Ridge, Volcán Ecuador on Isabela Island (Fig. 1). Such stress interactions are currently unknown and require future studies.

This study confirmed the expectation that Juana Ridge is dominated by Stage/Domain 2 of rift zone growth proposed by the Leslie et al. (2004) model out to a length of ~Km 10-15 from Capo Douglas. While the intrusive dike complex is likely well-developed only under the proximal ~5 km, it is clear much of the remainder of the rift zone is being built up by diking events, and thus propagating the dike complex to more distal regions. Stage/Domain 1 of the Leslie et al. (2004) may have been reactivated by the 1968 Fernandina caldera collapse. An important component to consider in future volcanic rift zone growth models is the early initiation of mass wasting events, which apparently precedes other characteristics of Stage/Domain 3 on Juana Ridge. This factor is important for comparisons of Puna Ridge and other Hawaiian rift zones to Juana Ridge and other Galápagos rift zones, in that Galápagos rift zone stress fields may favor submarine landsliding of a different nature than Hawaiian stress fields. This is not only important for understanding rift zone growth processes, but for tsunami hazard preparedness planning.

References

Allan, J. F., and T. Simkin. 2000. Fernandina Volcano's evolved, well-mixed basalts: Mineralogical and petrological constraints on the nature of the Galápagos plume. J. Geophys. Res. **105**: 6017-6041.

Cando, M., P. Arreaga, T. Toulkeridis, and G. de la Torre. 2006. Evidences for potential future sector collapse at Volcano Roca Redonda, northern Galapagos – tectonics, simulation and consequences. Program with Abstracts, Cities on Volcanoes **4:** 512.

Chadwick, W. W., and K. A. Howard. 1991. The pattern of circumferential and radial eruptive fissures on the volcanoes of Fernandina and Isabela islands, Galapagos. B. Volcanol. **53**: 259-275.

Chadwick, W. W., and J. H. Dieterich. 1995. Mechanical modeling of circumferential and radial dike intrusions on Galapagos volcanoes. J. Volcanol. Geoth. Res. **66:** 37-52.

Cougan, Allison. 2006. Process of sediment transport across the Galapagos Platform: A geophysical study of Canal Isabela. Unpublished Bachelor's Thesis, University of Washington.

Fialko, Y. A., and A. M. Rubin. 1999. What controls the along-strike slopes of volcanic rift zones? J. Geophys. Res. **104**: 20007-20020.

Fiske, R. S., and E. D. Jackson. 1972. Orientation and growth of Hawaiian volcanic rifts: the effect of regional structure and gravitational stresses. Proc. R. Soc. Lond. A. **329**: 299-326.

Fornari, D. J., M. D. Kurz, D. J. Geist, P. D. Johnson, G. Peckman, and D. Scheirer. 2001. New perspectives on the structure and morphology of the submarine flanks of Galapagos volcanoes—Fernandina and Isabela, Eos. Trans. AGU **82**: F1205.

Harpp, K. S., D. J. Fornari, D. Geist, and M. D. Kurz. 2003. Genovesa Submarine Ridge: A manifestation of plume-ridge interaction in the northern Galapagos Islands. Geochem. Geophys. Geosyst. **4**: 8511-8538.

Holcomb, R. T., J. G. Moore, P. W. Lipman, and R. H. Belderson. 1988. Voluminous submarine lava flows from Hawaiian volcanoes. Geology **16**: 400-404.

Kurz, M. D., and D. Geist. 1999. Dynamics of the Galapagos hotspot from helium isotope geochemistry. Geochim. Cosmochim. Acta **63**: 4139-4156.

Kurz, M. D., D. J. Fornari, J. M. Curtice, M. Perfit, D. Scheirer, and D. Geist. 2000. The Leading Edge of the Galapagos Hotspot: New Submarine Evidence from Fernandina Volcano. Eos. Trans. AGU **81**: F1282.

Kurz, M. D., D. J. Fornari, D. Geist, and the Shipboard Scientific Party. 2001. Cruise Report DRIFT Leg-4 R/V Roger Revelle. [Online] http://science.whoi.edu/galap_rv_drft4/index.html

Leslie, S. C., G. F. Moore, and J. K. Morgan. 2004. Internal structure of Puna Ridge: evolution of the submarine East Rift Zone of Kilauea Volcano, Hawai'i. J. Volcanol. Geoth. Res. **129**: 237-259.

Lonsdale, P. 1989. A geomorphological reconnaissance of the submarine part of the East Rift Zone of Kilauea Volcano, Hawaii. B. Volcanol. **51**: 123-144.

Malahoff, A., and F. McCoy. 1967. The Geologic Structure of the Puna Submarine Ridge, Hawaii. J. Geophys. Res. **72**: 541-548.

Moore, J. G., and W. W. Chadwick. 1995. Offshore Geology of Mauna Loa and Adjacent Areas, Hawaii, p. 21-44. *In* J. M. Rhodes and J. P. Lockwood [eds.], Mauna Loa Revealed: Structure, Composition, History, and Hazards. Amer. Geophys. Union Monogr.

Rowland, S. K. 1996. Slopes, lava flow volumes, and vent distributions on Volcan Fernandina, Galápagos Islands. J. Geophys. Res. **101**: 27,657–27,673.

Simkin, T., and K. A. Howard. 1970. Caldera Collapse in the Galápagos Islands, 1968. Science **169:** 429-437.

Smith, D. K., M. A. Tivey, P. M. Gregg, and L. S. L. Kong. 2001. Magnetic anomalies at the Puna Ridge, a submarine extension of Kilauea Volcano: Implications for lava deposition. J. Geophys. Res. **106:** 16,047-16,060.

Smith, D. K., L. S. L. Kong, K. T. M. Johnson, and J. R. Reynolds. 2002. Volcanic morphology of the submarine Puna Ridge, Kilauea Volcano, p. 125-142. *In* E. Takahashi, P.W. Lipman, M. O. Garcia, and S. Aramaki [eds.], Hawaiian Volcanoes: Deep Underwater Perspectives. Am. Geophys. Union Monogr.

Thompson, Wesley. J. 2006. A hydrographic search for hydrothermal fluids on the Juana Ridge, northwest Fernandina Island, Galápagos. Unpublished Bachelor's Thesis, University of Washington.

Table 1. TN189 (Leg 1) Juana Ridge Survey way-point locations and operations.

		Start			End	
Operation	South Latitude	West Longitude	Depth (m)	South Latitude	West Longitude	Depth (m)
CTD cast	00° 19.98’	91° 50.00’	3291			
Line 1	00° 19.98’	91° 50.00’	3289	00° 19.46’	91° 43.14’	2240
Line 2	00º 18.56’	91º 43.27’	1758	00º 17.12’	91º 49.17’	1650
Line 3	00º 14.24’	91º 49.50’	1725	00º 18.10’	91º 42.49’	1274
Line 4	00º 17.53’	91º 42.07’	870	00º 11.90’	91º 48.11’	3092
Line 5	00º 10.04’	91º 46.19’	2486	00º 16.60’	91º 41.80’	1099
Line 6	00º 16.31’	91º 41.07	1464	00º 09.13’	91º 43.50’	2479
Line 7	00º 09.06’	91º 39.99	3032	00º 13.84’	91º 40.00’	2370
Line 8	00º 13.84’	91º 40.01	2372	00º 20.74’	91º 45.17’	2985
Line 9	00º 21.30’	91º 44.32	2870	00º 14.03’	91º 39.00’	2315
Line 10	00º 14.53’	91º 38.22	2211	00º 21.86’	91º 43.67’	2718

Figure Captions

Figure 1. Map of the Galápagos Archipelago. Direction of movement of the Nazca Plate (on which the Galápagos Archipelago is built) is to the east. This results in the youngest Galápagos volcanism in the western portion of the archipelago. Box around Fernandina Island shows the area of Fig. 2. Genovesa Ridge is shown in the northeast. Background map courtesy of William Chadwick, Oregon State University.

Figure 2. Map of Fernandina Island showing distributions of circumferential and radial eruptive fissures (after Chadwick and Dieterich 1995). Circumferential eruptive fissures dominate around the volcanic summit crater and radial fissures dominate on the slopes of the volcano. The sub-aerial Fernandina Northwest Rift Zone is abbreviated to "FNWRZ" and its offshore continuation has been named Juana Ridge. The relationship of Fernandina Island to the Galápagos Archipelago is shown in Fig. 1. Background map courtesy of William Chadwick, Oregon State University.

Figure. 3. Dust clouds rising from Fernandina Island on July 4, 1968, three weeks after a major eruption in which the caldera floor dropped 300 m. Photo courtesy of Tom Simkin, Smithsonian Institution.

Figure 4. Proposed model for the evolution of a rift zone built adjacent to a mature volcanic flank. From Leslie et al. (2004), Fig. 9.

Figure 5. Survey track-lines throughout Leg 1 of R/V *Thomas G. Thompson* cruise TN189. The study area is shown by the box.

Figure 6. EM300 bathymetric map (gridded at 25 m resolution) showing location of cross-section profile segments A-A', B-B', C-C' and D-D' shown in cross-section view in Fig. 7. Segment E-E' (in white) is the track line along with the 3.5 kHz sub-bottom profile record in Fig. 8 was taken.

Figure 7. Cross-section view of profiles from Fig. 6: a) A-A' (2x vertical exaggeration) showing steepest slopes on the proximal ~2 km of the rift zone; b) B-B' (2.5x vertical exaggeration) showing a zone of high slope (11-12°) from 2100-2300 m water depth; c) C-C' (1.7x vertical

exaggeration) showing a well-defined axial profile for the proximal rift zone region d) D-D' (2.3x vertical exaggeration) showing an irregular axial profile for the distal rift zone region. Color scale is the same as in Fig. 6.

Figure 8. 3.5 kHz sub-bottom profile record along segment E-E' in Fig. 5 (12.5 x vertical exaggeration). Parabolic reflections indicate rough lava morphology, likely pillow basalt. No sediment reflections are apparent.

Figure 9. EM300 bathymetric map (gridded at 25 m resolution) with insets showing and quantifying the dimensions of volcanic and tectonic morphologies. Inset A: a field of craters and one sharp-sided cone, as well as a slump block related to mass wasting. Inset B: the most prominent slump block related to mass wasting in the study area. Inset C: Two prominent pit craters near the rift zone bend at Km 10. Inset D: A field of deep pit craters, which overly the high reflectivity lava flow fields in Fig. 10.

Figure 10. EM300 backscatter map. Dark gray is high reflectivity (lava) and light gray is lower reflectivity (sedimented areas). Red lines outline two prominent lava flow fields, which correspond with the area represented by Fig. 9, Inset D.

Figure 11. Magnetic anomaly map of the study area with contours in units of nano-Teslas. Study limits delimited by black lines. Double-dipole is evident by two prominent positive anomalies bracketing a negative anomaly overlying the rift zone axis.

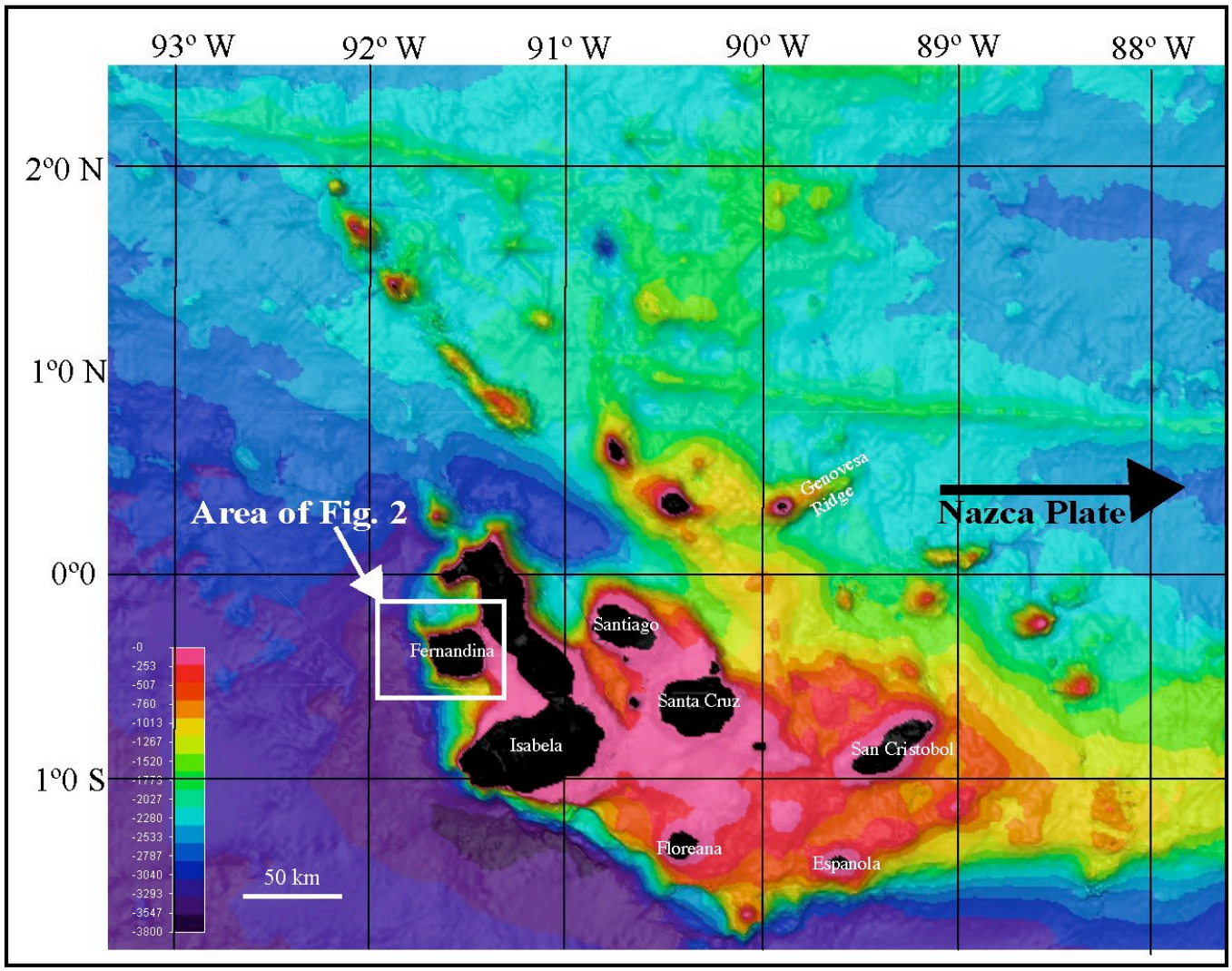

Jennifer Glass

Figure 1.

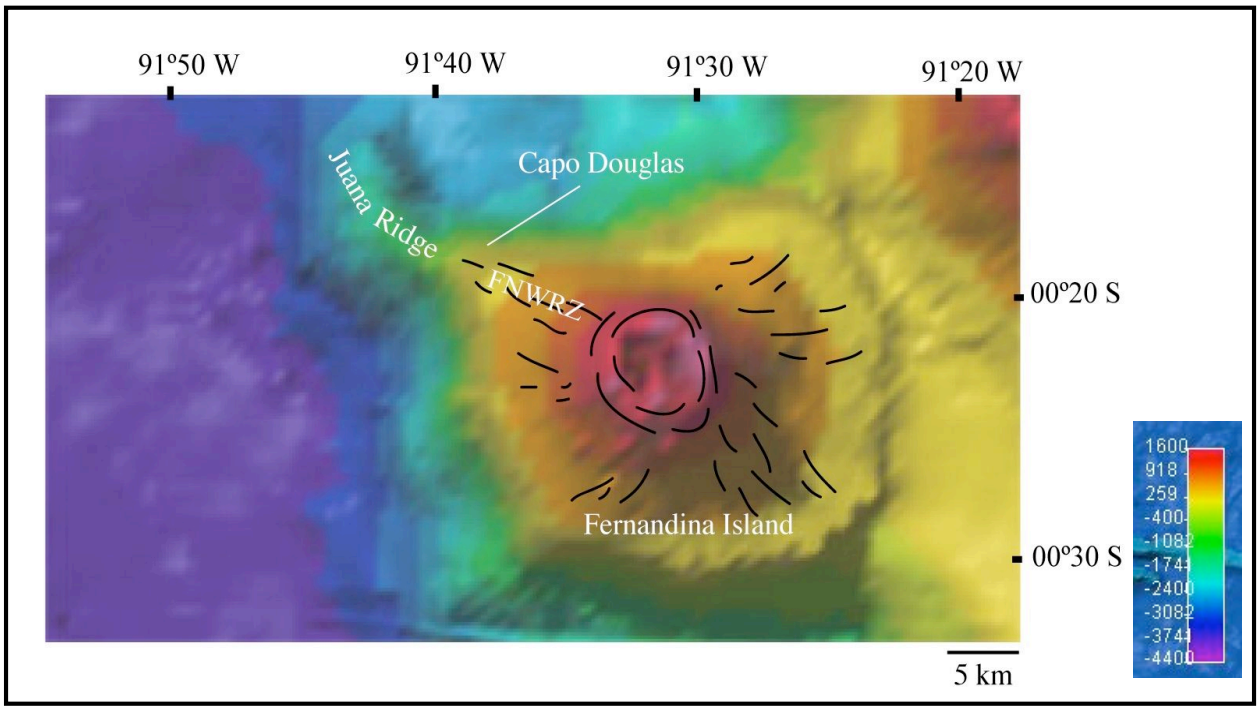

Jennifer Glass

Figure 2.

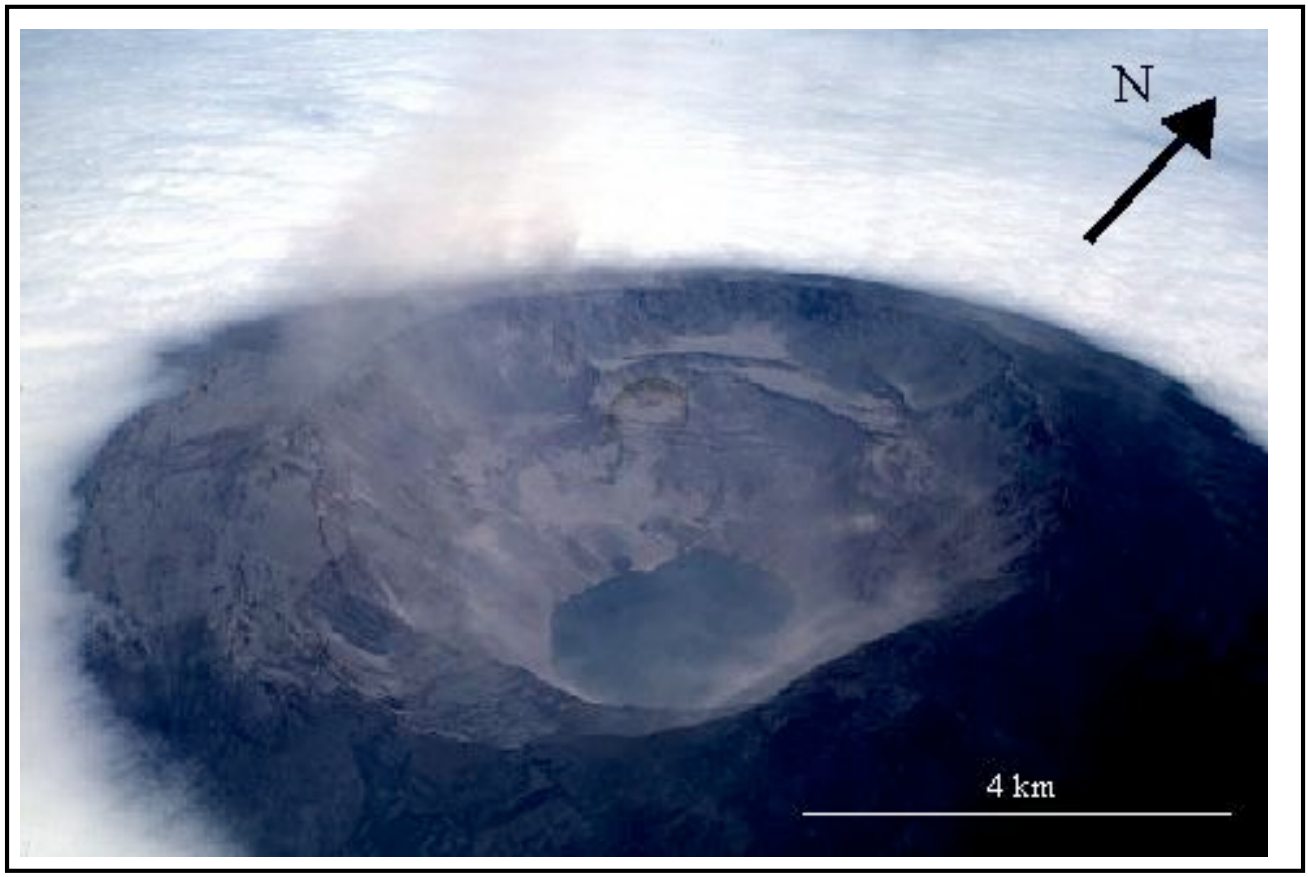

Jennifer Glass

Figure 3.

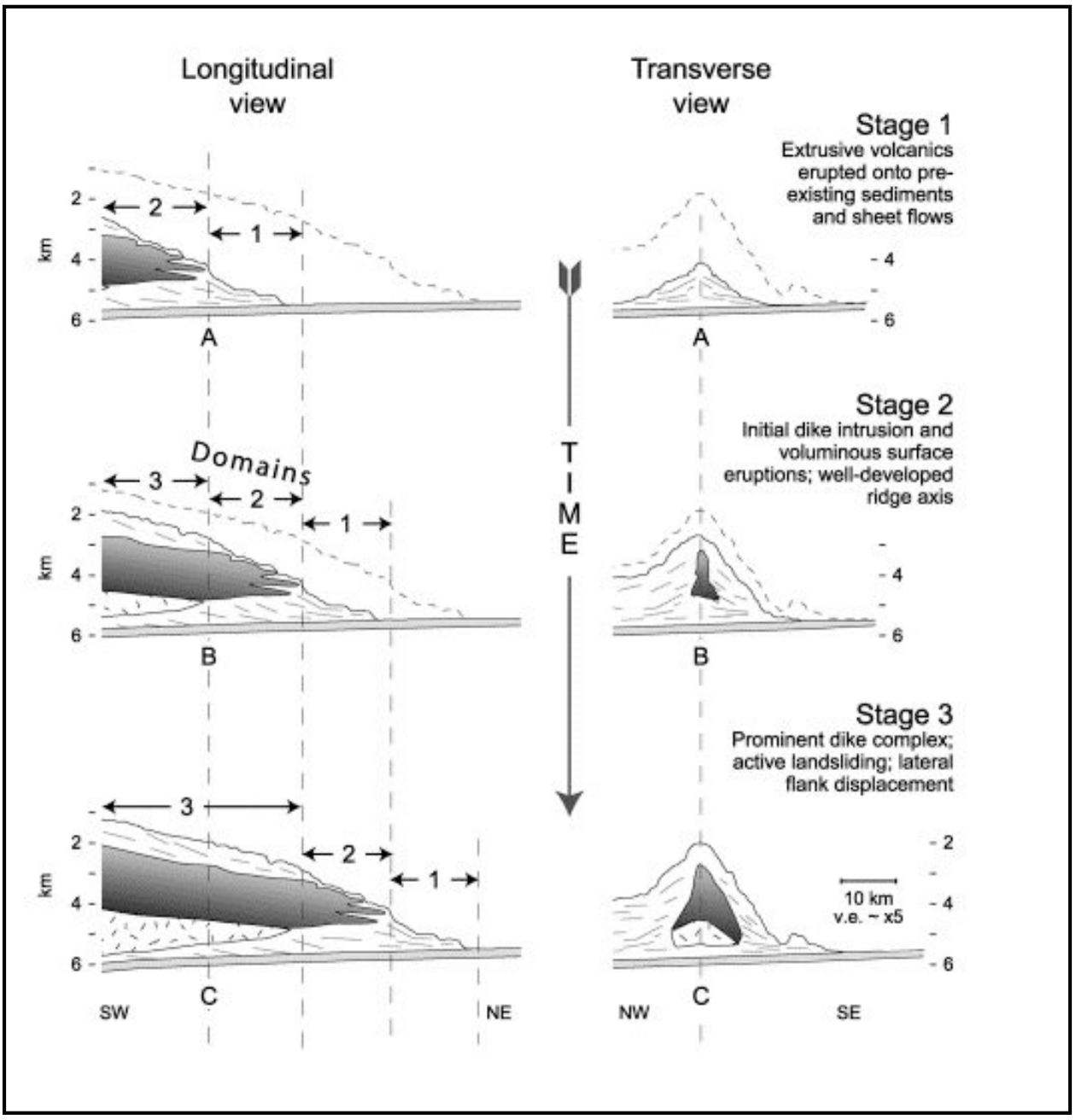

Jennifer Glass

Figure 4.

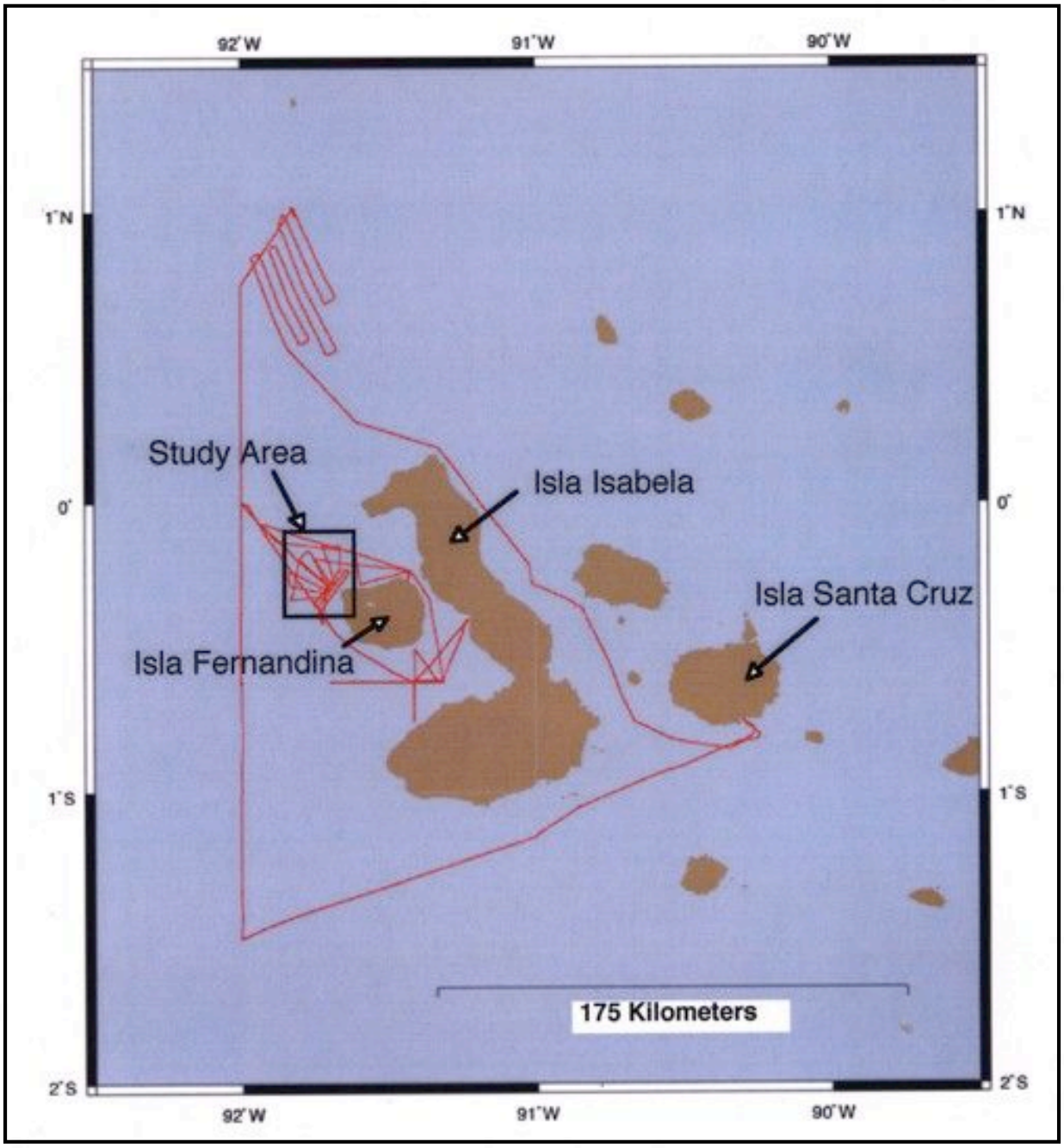

Jennifer Glass

Figure 5.

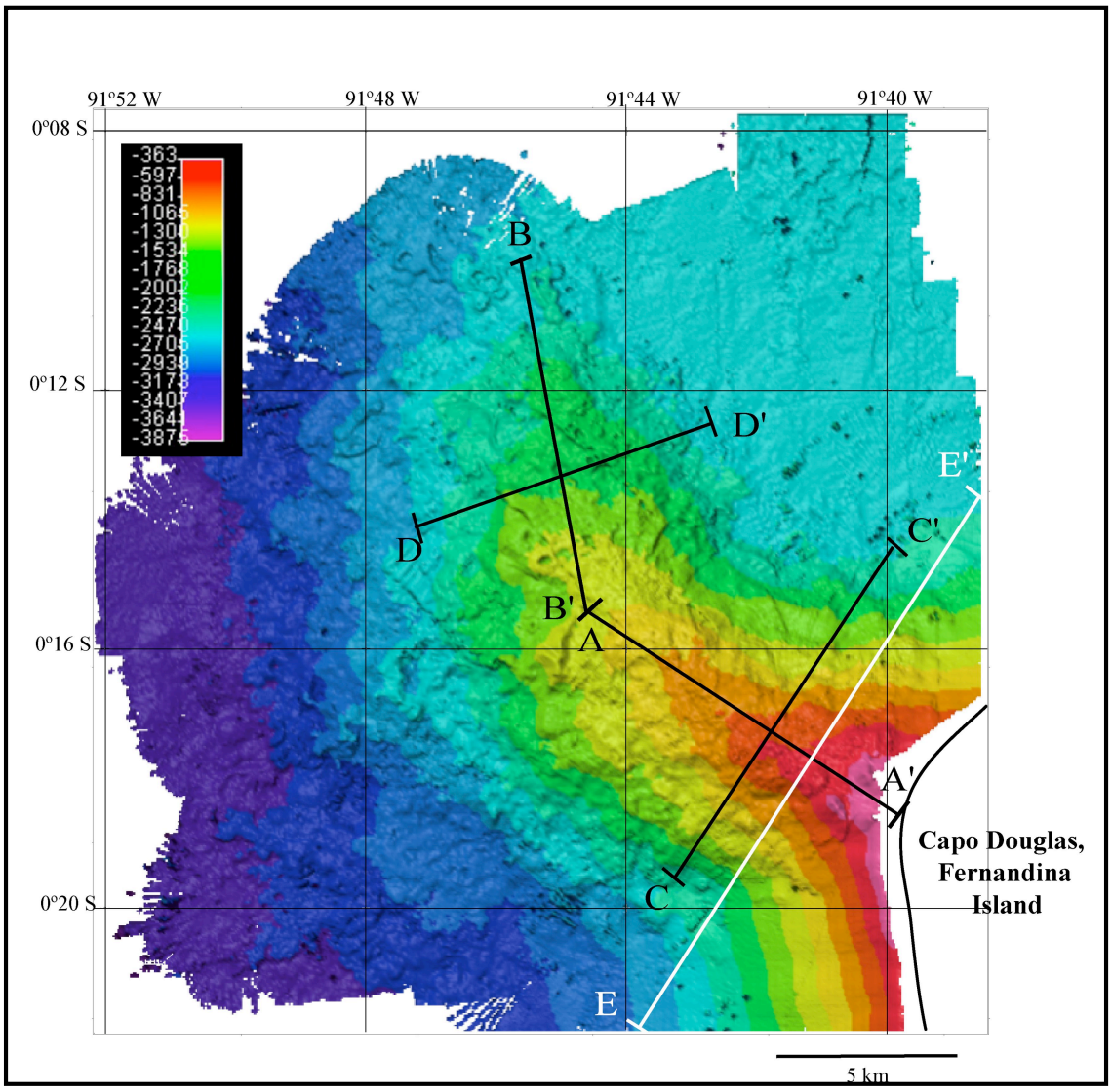

Jennifer Glass

Figure 6.

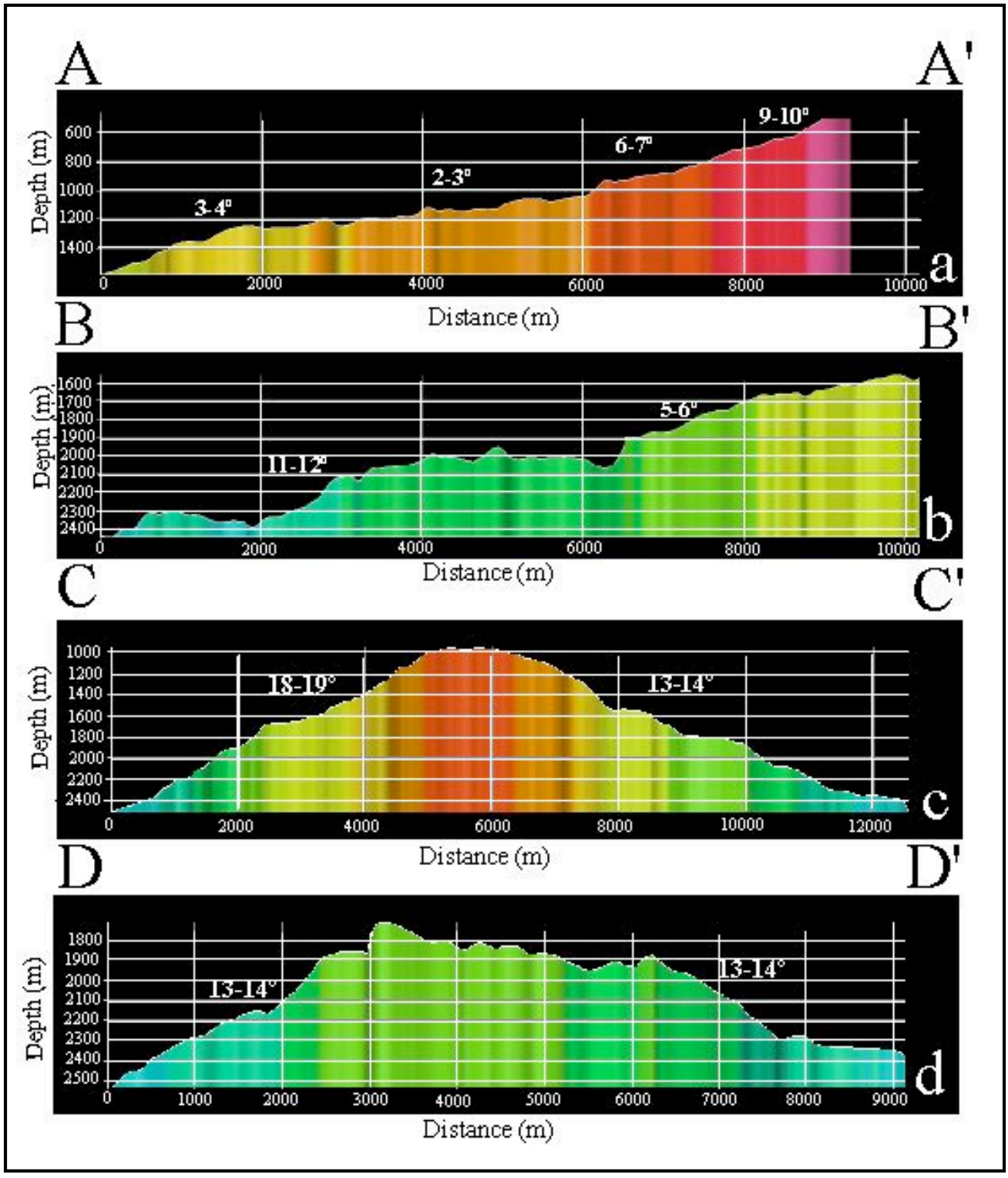

Jennifer Glass

Figure 7.

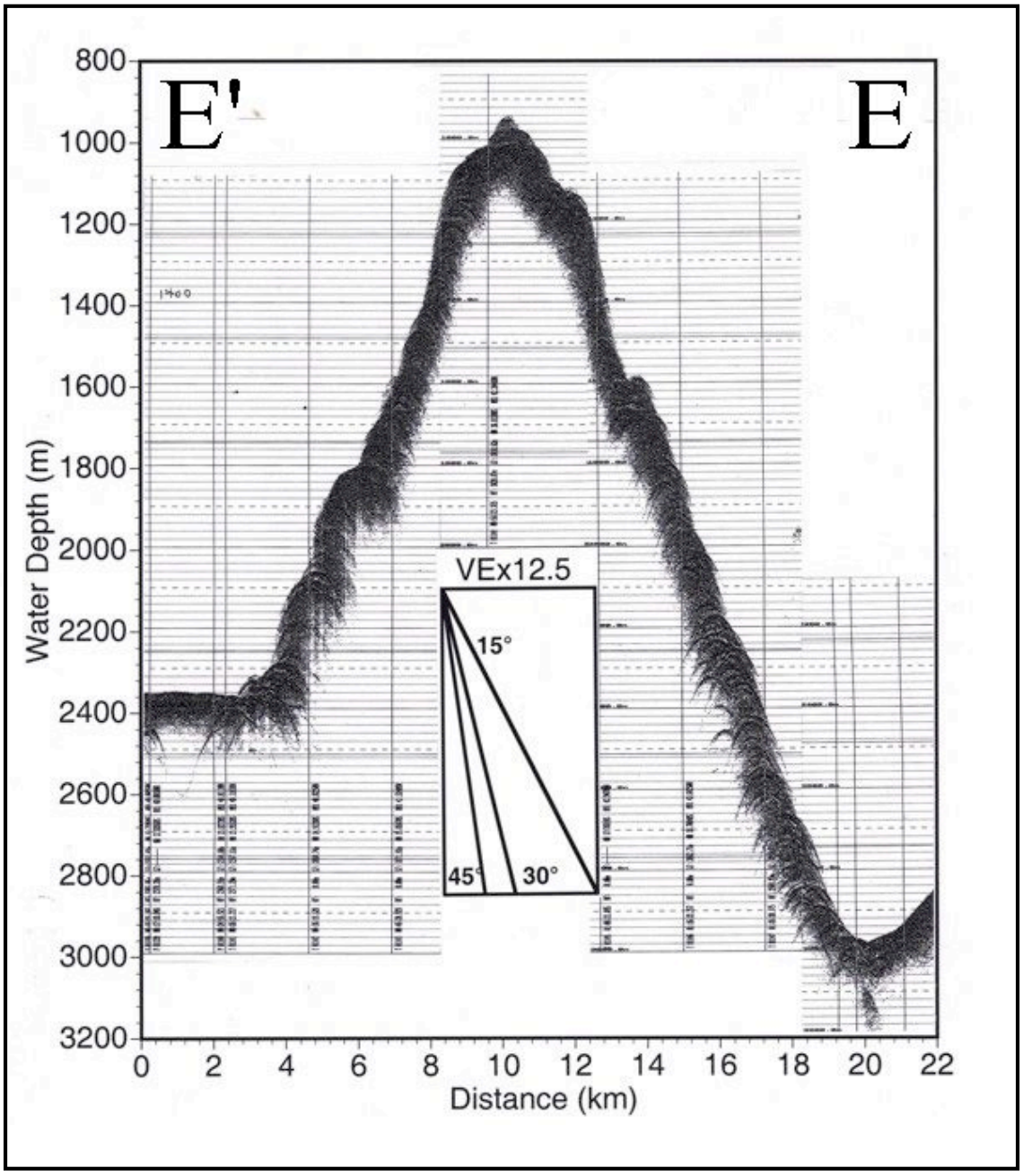

Jennifer Glass

Figure 8.

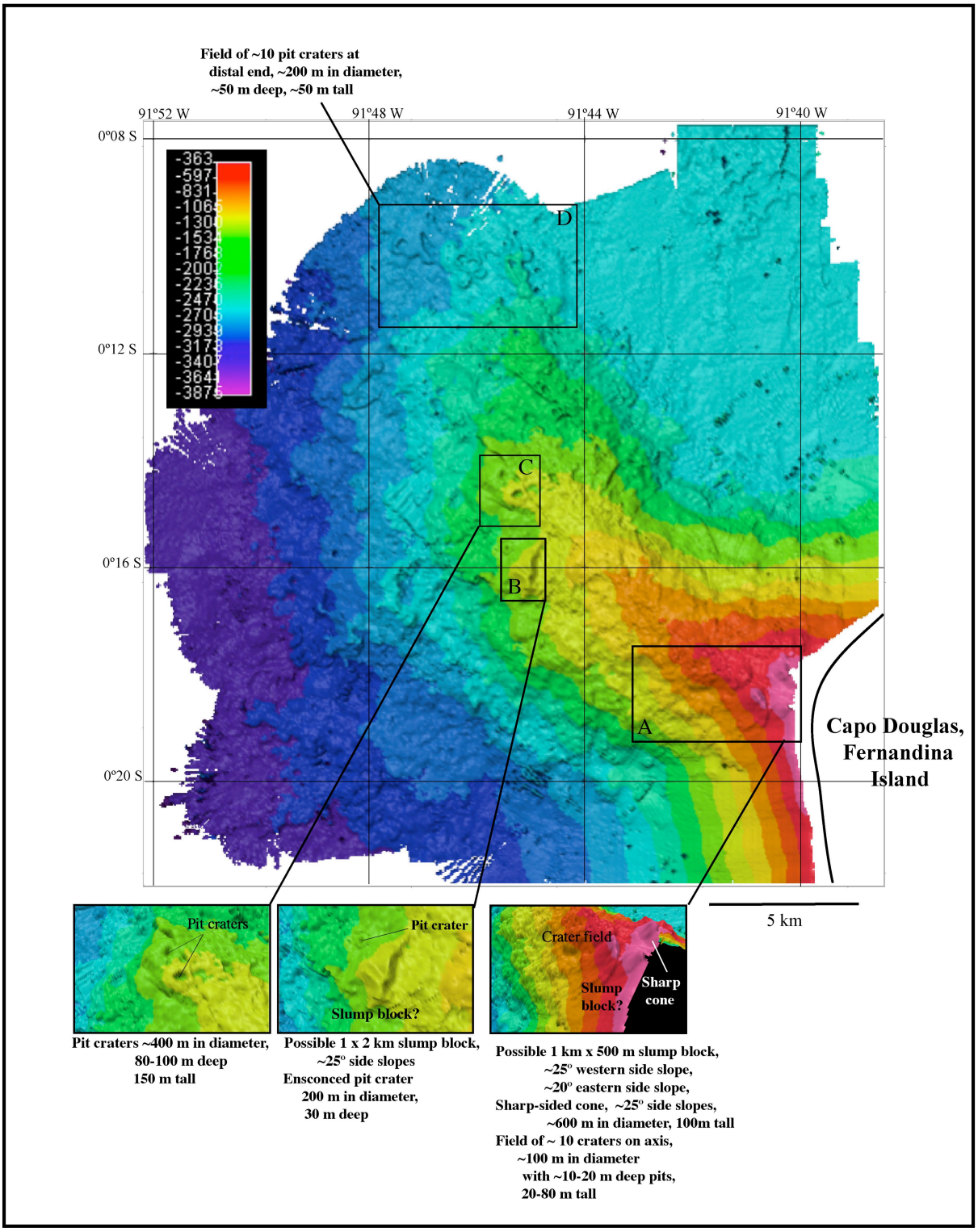

Jennifer Glass

Figure 9.

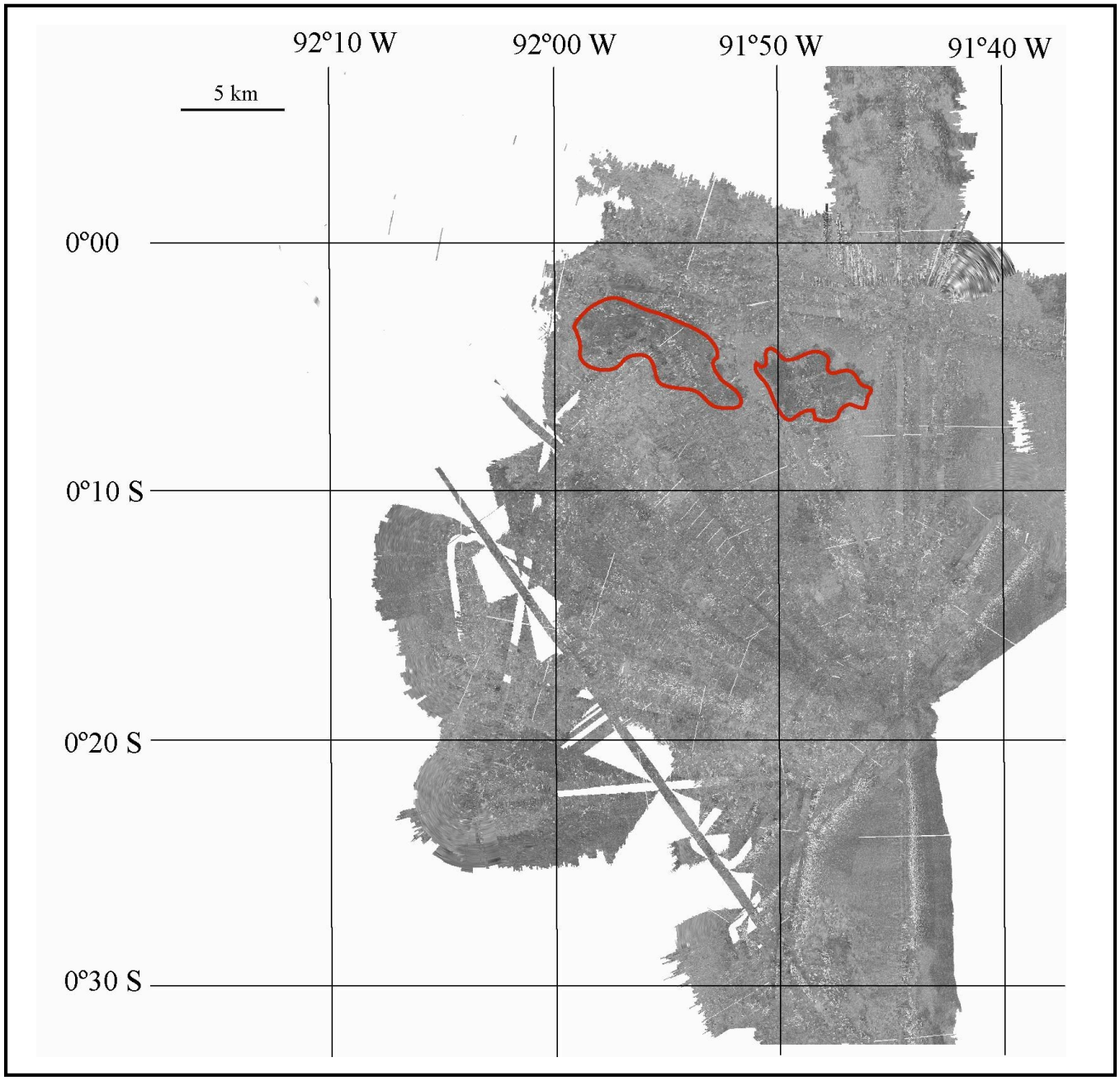

Jennifer Glass

Figure 10.

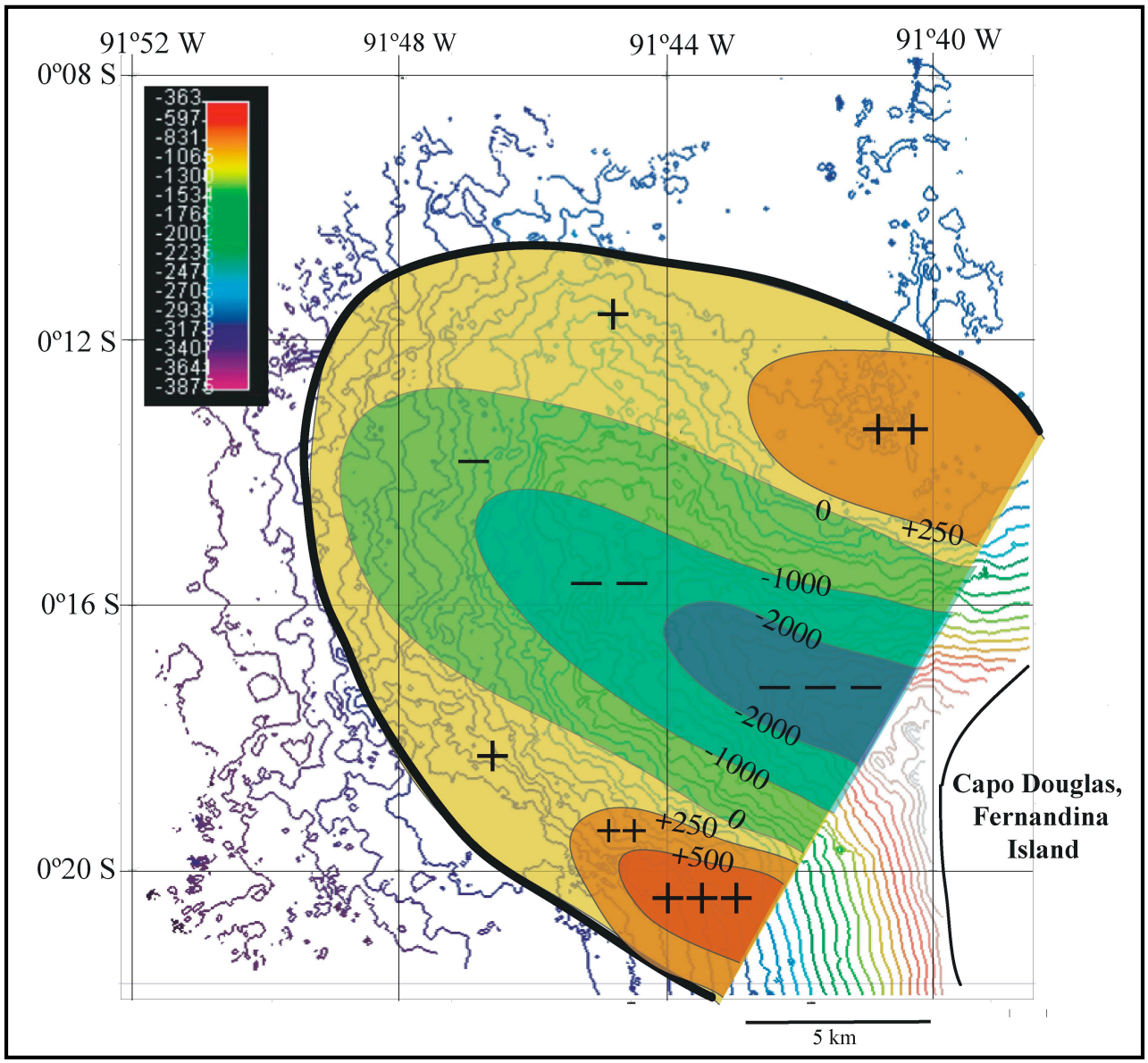

Jennifer Glass

Figure 11.